A High-Lift Building Block Flow: Turbulent Boundary Layer Relaminarization Final Report for NASA NAG4-206

Corey Bourassa, Graduate Research Assistant
Flint O. Thomas, Professor
Robert C. Nelson, Professor
Hessert Center for Aerospace Research
Department of Aerospace & Mechanical Engineering
University of Notre Dame
Notre Dame, IN 46556

July 25, 2001

1 Background & Motivation

1.1 Turbulent Boundary Layer Relaminarization & High-Lift Systems

In a high-lift system, there is evidence that relaminarization of the main element boundary layer may have an effect on the global aerodynamic behavior of the system. If one examines the effect of Reynolds number on $C_{L_{max}}$ of a high-lift system, experience dictates that for increasing Reynolds number $C_{L_{max}}$ would increase. In fact, this is not always the case as can be seen schematically in Figure 1, which demonstrates an example of $C_{L_{max}}$ behavior for a high-lift system. As one can see, the low Reynolds number region is approximately linear, but as Reynolds number increases $C_{L_{max}}$ decreases dramatically until at even larger Reynolds number it begins to increase again. This phenomena is referred to as the *Inverse Reynolds Number Effect* and its cause is unknown. The inverse Reynolds number phenomenon is dangerous when the designer extrapolates wind tunnel data performed at low Reynolds number to flight Reynolds number. The discrepancy in $C_{L_{max}}$ can be striking as is seen in $C_{L_{max}}$ data taken at the RAE wind tunnel using a semi-span high-lift model in Figure 2.

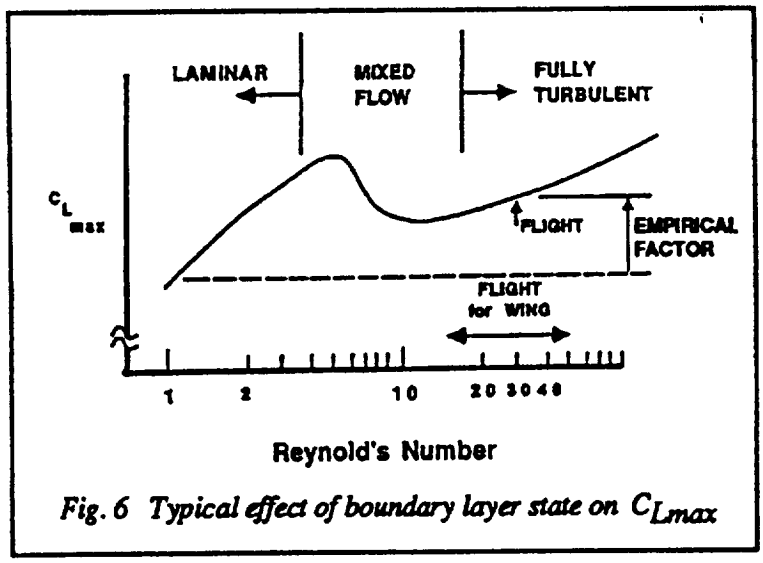

Fig. 6 Typical effect of boundary layer state on C_{Lmax}

Figure 1: Taken from Meredith, P.T., "Viscous Phenomena Affecting High-Lift Systems and Suggestions for Future CFD Development," AGARD CP-515, pp. 19-1, 19-8, 1993.

Flight test experiments on leading edge transition and relaminarization conducted by van Dam et al[1] using the NASA Transport Systems Research Vehicle, a Boeing 737-100, has provided tantalizing evidence, but not proof, that relaminarization may be responsible for the inverse Reynolds number effect that can occur at high Reynolds numbers. Relaminarization in high-lift systems may occur as the turbulent boundary layer proceeds from the attachment location, under the leading edge, around the nose of the main element. As the turbulent

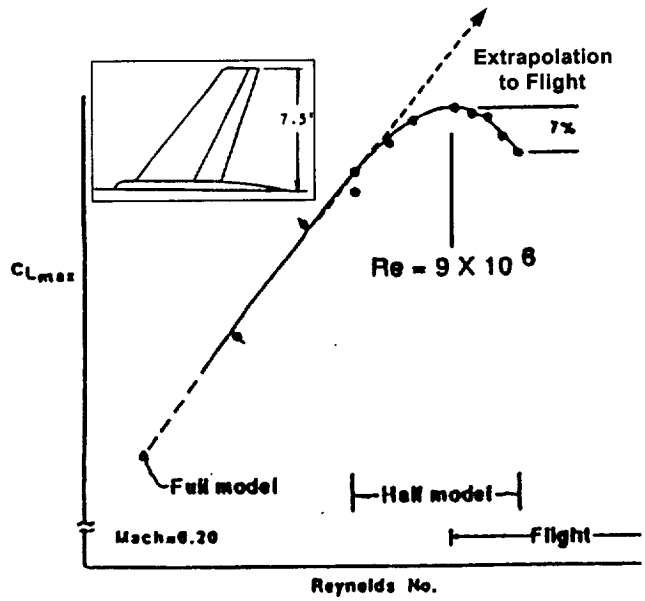

Figure 2: Semi-span high-lift model demonstrating the *Inverse Reynolds Number Effect.* Figure adapted from Mack & McMasters (1992).

boundary layer proceeds around the nose, it encounters a strong favorable pressure gradient. The accelerated boundary layer may then relaminarize; relaminarization would then thin the boundary layer from that of its previous turbulent state. A decrease in the main element boundary layer thickness will delay separation and have a favorable effect on $C_{L_{max}}$. High-lift research using the Trapezoidal Wing model conducted as part of the Advanced Subsonic Transport program at NASA Langley Research Center provided more evidence that relaminarization is present on high-lift systems. Infrared imaging of the upper-surface of the main element shows laminar-to-turbulent transition in Figure 3, while the attachment line Reynolds number was calculated to be well above the critical value for turbulent transition; this indicates the presence of reverse transition or relaminarization[2].

2 The University of Notre Dame's Turbulent Boundary Layer Relaminarization Test Facility

In order to better understand the flow physics associated with turbulent boundary layer relaminarization and develop appropriate tools to quantify the extent of relaminarization in high-lift systems, a fundamental study of relaminarization is underway at the University of Notre Dame's Hessert Center for Aerospace Research. A unique facility has been designed and constructed to investigate turbulent boundary layer relaminarization at Reynolds numbers not before reached in the laboratory environment. The Relaminarization Test Facility (RTF) is located in the Hessert Center's 1.5 m × 1.5 m (5 ft × 5 ft) atmospheric wind tunnel. The RTF, shown in Figures 4 and 5, has several unique features:

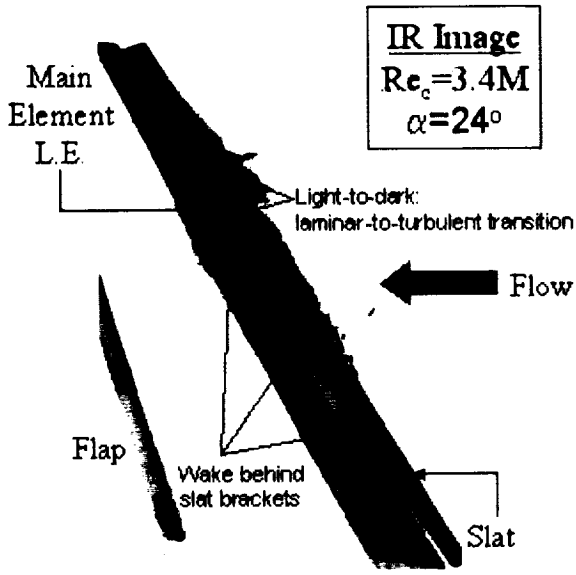

Figure 3: Infrared flow visualization image of the Trapezoidal Wing model showing laminar-to-turbulent transition on the upper-surface of the main element. Provided courtesy of Paul Johnson and The Boeing Co.

1. Operation at large Reynolds numbers (in excess of $\mathrm{Re}_\theta = 4500$),
2. A selectable *constant* K environment through the use of a adjustable linear wall contour ($0 \lesssim K \lesssim 5.0 \times 10^{-6}$),
3. A large boundary layer development region ($\sim 10\,\mathrm{m}$).

The previous year has been spent constructing, refining, and testing the RTF. Currently the RTF is operational and research efforts focus on documenting the boundary layer state both upstream and throughout the contraction region in which the turbulent boundary layer would be expected to relaminarize for $K \gtrsim 3.0 \times 10^{-6}$. Three test cases were identified for investigation prior to construction:

1. Case #1, $K = 5.0 \times 10^{-6}$,
2. Case #2, $K = 3.5 \times 10^{-6}$,
3. Case #3, $K = 1.0 \times 10^{-6}$.

Each case is differentiated by its wall angle with Case #1 having the largest angle or contraction ratio and Case #3 having the smallest. Case #1 was chosen first for investigation.

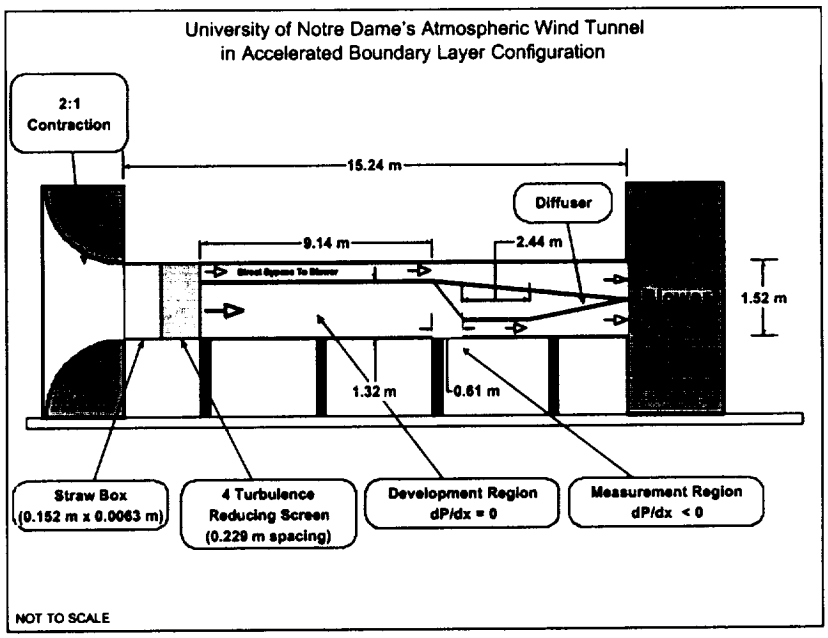

Figure 4: Schematic of the Relaminarization Test Facility (RTF) at the Hessert Center for Aerospace Research.

2.1 Results: Initial Conditions

The concept of the RTF is to subject a turbulent boundary layer to large flow accelerations. In order to draw comparisons between the effects of flow acceleration on each case listed above, it is desired to maintain a fixed boundary layer state prior to flow acceleration. In this manner, each case cited above will have the same initial conditions regardless of the contraction angle. The location of the initial boundary layer conditions was fixed by examining the pressure gradient in the wind tunnel. It was observed that the boundary layer experiences a nominally zero pressure gradient environment until 7.62 m downstream of the wind tunnel inlet where the flow begins to accelerate prior to entering the contraction. Thus the location of the initial conditions was chosen to be $\mathbf{x}_o = 7.62\,\mathrm{m}$. Upstream of the $\mathbf{x}_o$ location, the turbulent boundary layer develops under nominally zero pressure gradient conditions and thus all flow field measurements will be conducted downstream of this location. For comparison, the streamwise coordinate has been nondimensionalized by the contraction's streamwise length ($L = 0.6096\,\mathrm{m}$) and the upstream end of the contraction ($x_c = 9.14\,\mathrm{m}$) set to the "zero" location. Thus in all following data to be reported, the initial data location will be referred to as $\frac{x_o}{L} = \frac{7.62\,\mathrm{m} - 9.14\,\mathrm{m}}{0.6096\,\mathrm{m}} = -2.58$, the contraction's upstream location as $\frac{x}{L} = 0$, and the location of contraction's downstream end as $\frac{x}{L} = 1$.

Using a combination of X-wire and single-wire hot wire probes, the turbulent boundary layer state has been documented. For the $\frac{x_o}{L} = -2.58$ location, the mean streamwise component of velocity is plotted in Figure 6 and the fluctuating streamwise component of velocity is plotted in Figure 7. For reference, the data is plotted with the zero pressure gradient turbulent boundary layer data from Adrian, et al[3] at $\mathrm{Re}_\theta = 6845$, where θ is the

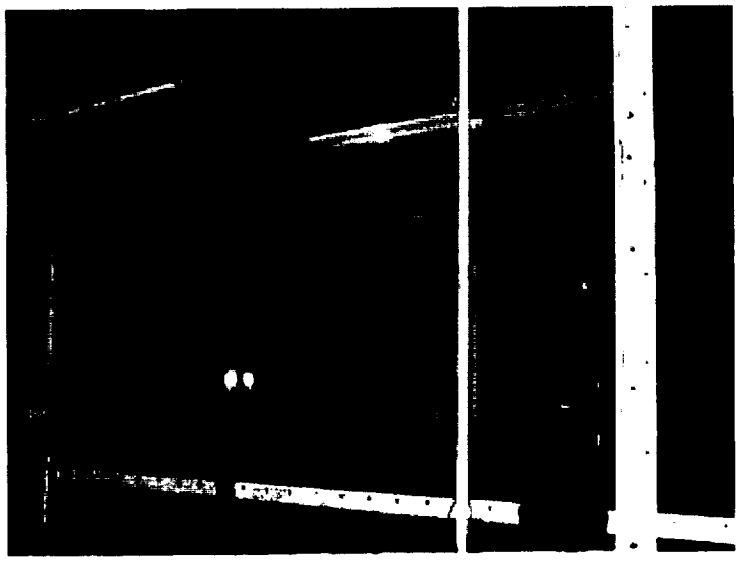

Figure 5: Photograph of the Relaminarization Test Facility (RTF) at the Hessert Center for Aerospace Research.

x_o [m]	δ [m]	δ^* [m]	θ [m]	H	Re_θ	Re_x	c_f	u_τ [$\frac{m}{s}$]
7.62	0.2007	0.0256	0.0195	1.31	4694	1.84×10^6	0.0029	0.143

Table 1: List of initial conditions for the turbulent boundary layer.

momentum thickness. Excellent agreement is seen in the mean and RMS profiles. The cause of the slight discrepancy in the RMS velocity profiles in the inner boundary layer has not been identified, but is believed to be of little consequence. From the mean velocity profile, the boundary layer parameters were computed and are listed for reference in Table 1, where δ is the boundary layer thickness, δ^* is the displacement thickness, H is the shape factor, c_f is the skin friction coefficient determined using Oil Film Interferometry, and u_τ is the friction velocity.

2.2 Results: Case #1

Using static pressure ports located in the tunnel floor, the pressure distribution of the Case #1 boundary layer (C1BL) was recorded. Figure 8 shows the C1BL distribution in addition to the theoretical pressure distribution for the linear contraction and the corresponding K values. The theoretical pressure distribution was calculated using 2D theory and deviation of the measured pressure distribution from theory is due to viscous effects. The peak value of the acceleration parameter occurs at $\frac{x}{L} = 0$ and has an average value of $K \sim 4.2 \times 10^{-6}$ throughout the contraction. The acceleration parameter does not achieve a constant value, but this is again due to the discrepancy between the measured and theoretical pressure distribution.

The skin friction distribution was measured for the C1BL using the oil film interferometry

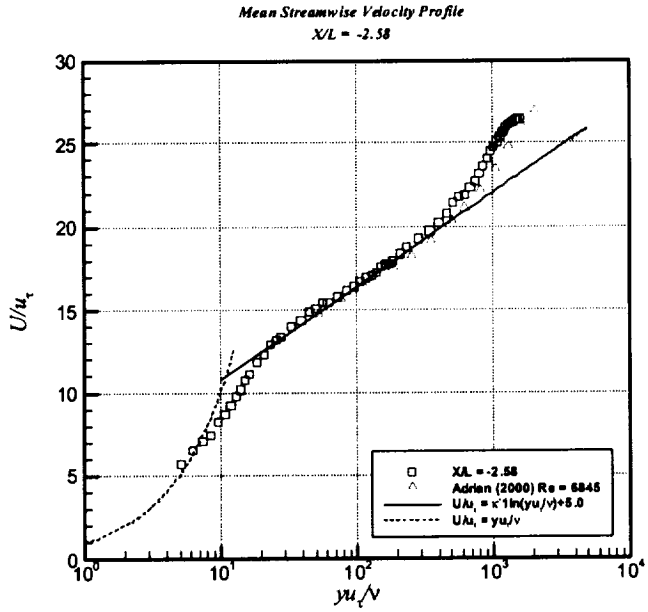

Figure 6: Mean streamwise component of velocity plotted in inner variables.

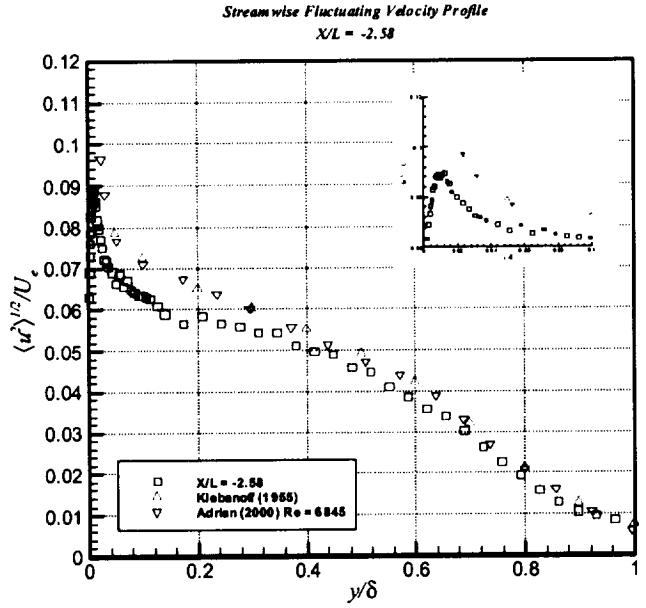

Figure 7: Fluctuating streamwise component of velocity plotted versus nondimensional height.

(OFI) technique. The skin friction distribution is shown in Figure 9. One can see the flow acceleration begins well upstream of the $\frac{x}{L} = 0$ location, which coincides with the increase in the skin friction coefficient. Just upstream of the contraction, the skin friction rises steeply and peaks just inside the contraction at $\frac{x}{L} = 0.125$ after which it rapidly declines. A decrease in the skin friction is consistent with relaminarization of the accelerated turbulent boundary layer. For reference, the laminar value of the skin friction coefficient at the end of the contraction and the "zero-pressure" gradient value (the value of the skin friction coefficient if the turbulent boundary layer were to reach that x location without acceleration) is shown labeled as "turbulent". The skin friction coefficient is an order of magnitude greater than the laminar value, but seems to reach a value consistent with the "turbulent" value.

3 Summary

At the completion of NASA NAG4-206, a working wind tunnel test facility has been constructed at the University of Notre Dame's Hessert Center. The relaminarization test facility has been constructed in the 1.5 m × 1.5 m (5 ft × 5 ft) atmospheric wind tunnel and generates a $\mathrm{Re}_\theta = 4694$ turbulent boundary layer in nominally zero-pressure gradient before it is exposed to the Case #1 pressure gradient ($K \sim 4.2 \times 10^{-6}$), which is believed to be sufficient to achieve relaminarization. Future work to be conducted will include measuring the response of the turbulent boundary layer to the favorable pressure gradients created in the test facility and documenting this response in order to understand the underlying flow physics responsible for relaminarization. It is the goal of this research to have a better understanding of accelerated turbulent boundary layers which will aid in the development of future flow diagnostic utilities to be implemented in applied aerodynamic research.

4 References

References

[1] C.P. van Dam, P.M.H.W. Vijgen, L.P. Yip, and R.C. Potter. Leading-edge transition and relaminarization phenomena on a subsonic high-lift system. *AIAA*, Paper No. 93–3140, 1993.

[2] Jones K.M. Johnson, P.L. and M.D. Madson. Experimental investigation of a simplified 3d high lift configuration in support of CFD validation. *AIAA Paper 2000-4217*, 2000.

[3] R.J. Adrian, C.D. Meinhart, and C.D. Tomkins. Vortex organization in the outer region of the turbulent boundary layer. *Journal of Fluid Mechanics*, 422:1–54, 2000.

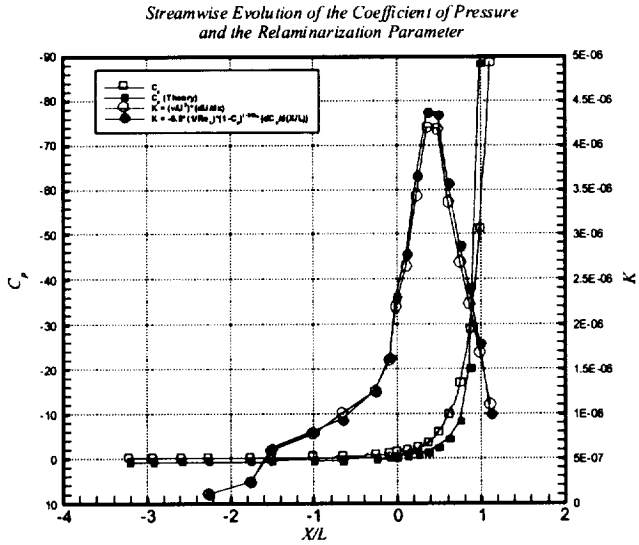

Figure 8: Case #1 C_P distribution through the linear contraction. In addition, the theoretical C_P distribution and corresponding K values are shown for reference.

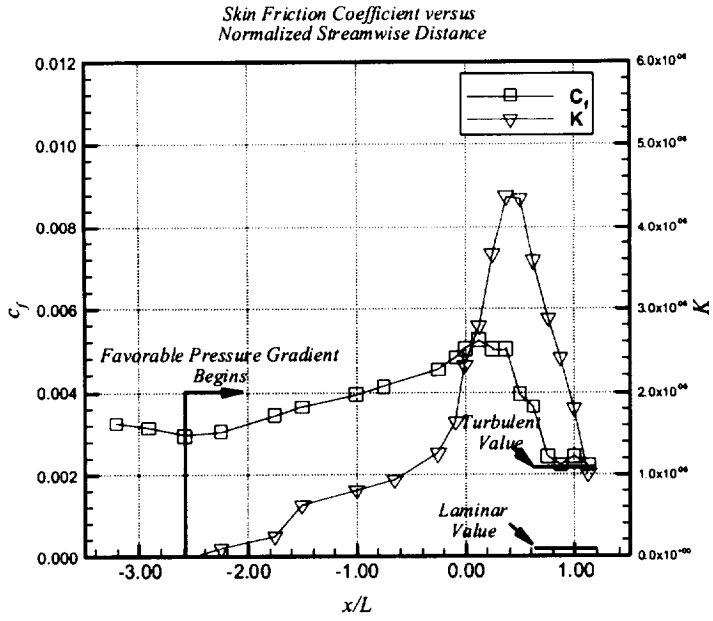

Figure 9: Case #1 skin friction distribution upstream and through the linear contraction.